Clays and Clay Minerals, Vol. 61, No. 1, 1–10, 2013.

INFLUENCE OF CATIONS ON AGGREGATION RATES IN Mg-MONTMORILLONITE

AL. KATZ[1], MIN XU[2], JEFFREY C. STEINER[3], ADRIANNA TRUSIAK[3], ALEXANDRA ALIMOVA[4], PAUL GOTTLIEB[4], AND KARIN BLOCK[3,*]

[1] Department of Physics, City College of New York, New York, NY 10031, USA
[2] Department of Physics, Fairfield University, Fairfield, CT 06824, USA
[3] Department of Earth and Atmospheric Science, City College of New York, New York, NY 10031, USA
[4] Sophie Davis School of Biomedical Education, City College of New York, New York, NY 10031, USA

Abstract—Critical-zone reactions involve inorganic and biogenic colloids in a cation-rich environment. The present research defines the rates and structure of purified Mg-montmorillonite aggregates formed in the presence of monovalent (K^+) and divalent (Ca^{2+}, Mg^{2+}) cations using light-extinction measurements. Time evolution of turbidity was employed to determine early-stage aggregation rates. Turbidity spectra were used to measure the fractal dimension at later stages. The power law dependence of the stability ratios on cation concentration was found to vary with the reciprocal of the valence rather than the predicted reciprocal of valence-squared, indicating that the platelet structure may be a factor influencing aggregation rates. The critical coagulation concentrations (CCC) (3 mM for $CaCl_2$, 4 mM for $MgCl_2$, and 70 mM for KCl) were obtained from the stability ratios. At a later time and above a minimal cation concentration, turbidity reached a quasi-stable state, indicating the formation of large aggregates. Under this condition, an approximate turbidity forward-scattering correction factor was applied and the fractal dimension was determined from the extinction spectra. For the divalent cations, the fractal dimensions were 1.65 ± 0.3 for Ca^{2+} and 1.75 ± 0.3 for Mg^{2+} and independent of cation concentrations above the CCC. For the monovalent cation, the fractal dimension increased with K^+ concentration from 1.35 to 1.95, indicating a transition to a face-to-face geometry from either an edge-to-edge or edge-to-face orientation.

Key Words—Aggregation Rates, Critical Coagulation Concentration, Fractal Dimension, Montmorillonite, Smectite, Stability Ratio, Turbidity.

INTRODUCTION

The aggregation of colloidal clay particles is of widespread interest to industry and terrestrial ecology. Remediation applications often depend on manipulating conditions that lead to clay aggregation and aggregate stability (Kornilovich *et al*., 2005; Ravera *et al*., 2006). In the critical zone and in ecologic setting, clays play an important role in the interaction of inorganic nutrients, RNA, and proteins with dissolved organic compounds, soil clots, and other components of natural systems (Lagaly, 2006). The ubiquity of dissolved cations in the environment is a pivotal factor to understanding the aggregation rate, specific structure, and overall cohesiveness of aggregates and, therefore, dictates sequestration rates of suspended and dissolved species into sediment beds.

During aggregation, colloidal particles form a mass fractal structure (Meakin, 1983) at a rate determined by the potential barrier between particles. In the DLVO model (Derjaguin and Landau, 1941; Verwey and Overbeek, 1948), the potential is the sum of the attractive van der Waals potential and the repulsive Coulomb potential. The Coulomb potential, Ψ, decreases exponentially with distance, x, from the platelets, *i.e.* $\Psi \propto \exp(-\kappa x)$, where κ is the Debye-Hückel parameter and $1/\kappa$ is a measure of the double layer thickness (Hunter, 1993). The thickness of the electrical double layer is inversely proportional to the cation valence and the square root of the cation concentration (Luckham and Rossi, 1999). In distilled water or at low electrolyte concentrations, the charged double layer extends for several tens of nanometers and the energy barrier is much greater than k_BT where k_B is the Boltzmann constant and T is the absolute temperature. In order to aggregate, particles must overcome this energy barrier and, therefore, multiple collisions are necessary for particle adhesion. This regime is referred to as reaction limited colloidal aggregation (RLCA) or slow aggregation. At elevated cation concentration the double layer thickness decreases causing the potential barrier to also decrease, thus augmenting the probability of particle cohesion. At sufficiently high cation concentrations, the energy barrier disappears and every collision results in particle adhesion. This is the diffusion limited colloidal aggregation (DLCA) or fast aggregation regime. The concentration at which the energy barrier disappears is referred to as the critical coagulation concentration (CCC). The Schulze-Hardy rule predicts that the CCC varies with the valence of the coagulating ion raised to the sixth power (Hunter, 1993).

Smectites are highly reactive, expandable, negatively charged, hydrous 2:1 layered phyllosilicates; mont-

* E-mail address of corresponding author:
kblock@ccny.cuny.edu
DOI: 10.1346/CCMN.2013.0610101

morillonite is the common dioctahedral smectite (aluminous) clay mineral. While the theory for clustering within colloids is well understood, aggregate formation within clay minerals is less well defined and the derivation of accurate aggregation rates remains a challenge. In fact, van Oss *et al*. (1990) applied electrophoresis measurements to determine that DLVO theory does not adequately describe the flocculation of a smectite in NaCl solution and that polar forces must be included to explain the data for smectite. Individual clay-mineral platelets are conceptually assumed to be disk shaped with diameters of several hundred nm and thicknesses up to 5 nm (Plaschke *et al*., 2001; Tournassat *et al*., 2003; Ploehn and Liu, 2006). Platelet edges have a pH-dependent positive charge while the faces are negatively charged. This distribution of charge influences the structure of the aggregates and makes aggregation rates strongly dependent on cation valence and concentration. Three modes of smectite flocculation are possible (van Olphen, 1977; Keren and Sparks, 1995; Luckham and Rossi, 1999): (1) edge-to-face (E-F) aggregates in which the edge of a platelet associates with the face plane of another platelet; (2) face-to-face (F-F) aggregates formed by the association of parallel planes of platelets; and (3) edge-to-edge (E-E) aggregates formed by association of platelets along their edges. E-F aggregation occurs at lower cation concentration while at greater cation concentration F-F aggregation dominates (Stawiński *et al*., 1990; Keren and Sparks, 1995).

The aggregation kinetics and the role of electrolytes and/or pH in aggregation have been investigated for different clay minerals, including kaolinite, smectite, and illite (Ferreiro and Helmy, 1974; Novich and Ring, 1984; Goldberg and Glaubig, 1987; Stawiński *et al*., 1990; Goldberg *et al*., 1991; Pierre and Ma, 1999; Derrendinger and Sposito, 2000; Tawari *et al*., 2001; Lagaly and Ziesmer, 2003; Berka and Rice, 2004, 2005; Morris and Żbik, 2009; Nasser and James, 2009). In each of the studies listed, some aspect of CCC, fractal dimension, and sticking probability has been examined, though these studies have not applied turbidity measurements to ascertain aggregation rates and aggregate mass fractal dimension. In natural systems where clay minerals are suspended in complex solutions containing salts, organic compounds, and microbes, aggregation kinetics may have significant implications for carbon storage and pollutant transport (e.g. von Wachenfeldt *et al*., 2009; Bouchelaghem and Jozja, 2009). Time-resolved optical measurements allow one to probe the dynamics of clay colloidal stability for different environmental scenarios. Turbidity measurements provide information as to aggregate size, fractal dimension, and aggregation rates.

In the work presented here, the influence of Ca^{2+}, Mg^{2+}, and K^{+} cations on smectite flocculation were investigated over two time frames. At an early time, flocs were much smaller than optical wavelengths ($kr << 1$, where $k = 2\pi/\lambda$ is the optical wavenumber and r is the aggregate radius) and forward scattering can be ignored ($\gamma \approx 0$, in equation 5). In this situation, the turbidity $\tau \propto N$, where N is the number of primary particles per aggregate (Berry and Wills, 1986) and is also linear in time, leading to estimates for aggregation rates from the slope of $d\tau/dt$. At later times, when flocs were large ($kr >> 1$), the forward scattering correction factor lent itself to an approximation which allowed the fractal dimension to be extracted from the wavelength dependence of the turbidity.

MATERIALS AND METHODS

Accofloc® montmorillonite

A high-purity Na-montmorillonite (referred to by the commercial name 'Accofloc®' and with the chemical formula: $(Na,Ca)_{0.33}(Al_{1.67}Mg_{0.33})Si_4O_{10}(OH)_2n(H_2O)$; American Colloid Company, Arlington Heights, Illinois, USA) was processed as described below to obtain <0.2 μm clay particles and made homoionic with Mg^{2+} using the cation substitution technique described by Moore and Reynolds (1997). The Accofloc® was initially washed in 5% sodium hypochlorite (bleach) to remove organic contaminants and then triple washed in distilled water to rinse out the bleach. Large particles and non-clay minerals were removed by centrifugation at 3600 rpm (2700 g) for 20 min. This process resulted in the elimination of particles >0.2 μm (Moore and Reynolds, 1997; Środoń, 2006) and the supernatant comprising the <0.2 μm size fraction was collected for further optical analysis. The purified clay mineral was suspended in 0.1 M $MgCl_2$ overnight and centrifuged at 1300 rpm for 30 min and rinsed in distilled water 8–10 times. Two drops of $AgNO_3$ were added to the suspension after the rinses to verify that all chloride had been removed. The suspension was then autoclaved to ensure sterility. The concentration (w/v) of the stock suspension was 3.1 g/L in the $MgCl_2$ and $CaCl_2$ experiments and 2.2 g/L in the KCl experiments, as determined by light extinction and confirmed by drying and weighing. Visual inspection of the Accofloc® suspension confirmed the absence of noticeable aggregation during storage.

Light-extinction measurements

Light-extinction measurements were performed by first preparing suspensions of KCl, $CaCl_2$, and $MgCl_2$ in distilled water. Salt concentrations ranged from 0.2 mM to 1000 mM. Two mL of salt solution was placed in a 1 cm path-length quartz cuvette and the transmission integrated for 60 s to provide a reference signal. Next, 0.5 mL of Accofloc® suspension was added to the cuvette and the post-mixing transmission measured over a time period of 3000 s. This procedure resulted in a five-fold dilution of the Accofloc® and a 0.8-fold

https://doi.org/10.1346/CCMN.2013.0610101 Published online by Cambridge University Press

dilution of the salt solution. The Accofloc® concentration was sufficiently dilute so as to be in the single scattering region. Addition of the salts had no significant effect on the pH, which remained neutral. Specimens were illuminated by a halogen lamp coupled to an optical fiber. The transmitted light was collected by a second fiber coupled to a spectrometer (Ocean Optics) and computer. A 1 mm aperture was placed on the collection fiber coupler which was located 5 cm from the sample. This geometry limited the collection solid angle to 0.001 sr (steradian). A magnetic stirrer was used to prevent settling of the clay mineral aggregates during data collection. Experiments were performed at room temperature (20ºC) and at pH = 7. Spectra were integrated for 1 s intervals and each spectrum was saved separately. Spectra were analyzed in the 420 to 950 nm range, a region in which the Accofloc® optical absorption was negligible and light extinction was due entirely to scattering. The lack of structure in the extinction spectrum of Accofloc® in distilled water (not shown) confirmed that absorption is negligible at the wavelengths used in the data analysis (Banin and Lahav, 1968).

RESULTS AND DISCUSSION

Turbidity and aggregation

The early stages of clay mineral aggregation can be described by a bimolecular reaction process in which the kinetics is dominated by joining of individual particles (García-García *et al*., 2006, 2007): $N' + N' \rightarrow N_2'$. The rate equation can be written as:

$$\frac{dN'(t)}{dt} = -KN'^2(t) \tag{1}$$

where $N'(t)$ is the particle concentration and K is the aggregation rate per particle concentration. Integration of equation 1 gives:

$$\frac{1}{N'(t)} = \frac{1}{N'_0} + Kt \tag{2}$$

where N'_0 is the density of particles at $t = 0$. The average number of primary particles in an aggregate is $N = N'_0/N'(t)$ and thus

$$N(t) = 1 + KN'_0 t \tag{3}$$

From equation 3, in this early growth region, aggregate growth is linear in time (Puertas and Nieves, 1997; Kobayashi and Ishibashi, 2011).

Colloidal aggregates form a mass fractal structure in which the number of primary particles per aggregate is proportional to r^{D_f} where D_f is the fractal dimension of the aggregate and r is the aggregate radius of gyration. In the DLCA regime, aggregates have a fractal dimension in the range of 1.7 to 1.9, while in the RLCA regime, the fractal dimension ranges from 2.1 to 2.3 (Lin *et al*., 1989, 1990a, 1990b). Static light scattering techniques are frequently employed for measuring D_f (Sorensen, 2001). Recently, broadband light scattering was demonstrated to be useful in the investigation of $D_f(t)$ with ~1 s time resolution (Alimova *et al*., 2009). Both aggregate size and fractal dimension could be obtained from the spectral dependence of the turbidity in light-extinction measurements. The advantage of turbidity measurements over angle-resolved scattering spectroscopy is the potential to determine the aggregate size and related growth rates as well as the fractal dimensions of aggregates. The turbidity (τ) for a system of colloidal aggregates was given by (M. Xu, in prep.):

$$\tau = N'NLc_0k^4a^6\frac{2N}{(D_f-1)(D_f-2)}\frac{1}{(kr)^2}\left[1-(1+(kr)^2)^{1-D_f/2}\cos\big((D_f-2)\arctan(kr)\big)\right] \tag{4}$$

where L is the optical path length; $c_0k^4a^6$ is the scattering cross-section of a single platelet; a is the effective primary particle radius; D_f is the fractal dimension of the aggregate; and r is the radius of the aggregate. Note that $N'N$ is the number density of clay platelets and is a constant for each individual experiment.

The large extent of forward scattered light from clay mineral aggregates requires a correction to the Beer-Lambert law (Spinrad *et al*., 1978; Wind and Szymanski, 2002). The correction factor depends on the aggregate size as larger particles exhibit greater forward scattering. The turbidity correction factor, γ, is given by equation 5, below, where I_s is the total scattered light intensity and θ is the beam divergence. The relationship between the true transmitted intensity, I_T, and the measured transmitted intensity, I_M, is given by:

$$I_T = \frac{I_M - \gamma I_0}{1-\gamma} \tag{6}$$

where I_o is the source intensity. The turbidity corrected for forward scattering is given by:

$$\tau = \ln\left(\frac{I_T}{I_0}\right) = \ln\left(\frac{\frac{I_M}{I_0}-\gamma}{1-\gamma}\right) \tag{7}$$

$$\gamma = \frac{I_s(\theta)}{I_s} = \frac{1-\left[1+(kr)^2\sin^2(\theta/2)\right]^{1-D_f/2}\cos\left[(D_f-2)\arctan(kr\sin(\theta/2))\right]}{1-\left(1+(kr)^2\right)^{1-D_f/2}\cos\big((D_f-2)\arctan(kr)\big)} \tag{5}$$

https://doi.org/10.1346/CCMN.2013.0610101 Published online by Cambridge University Press

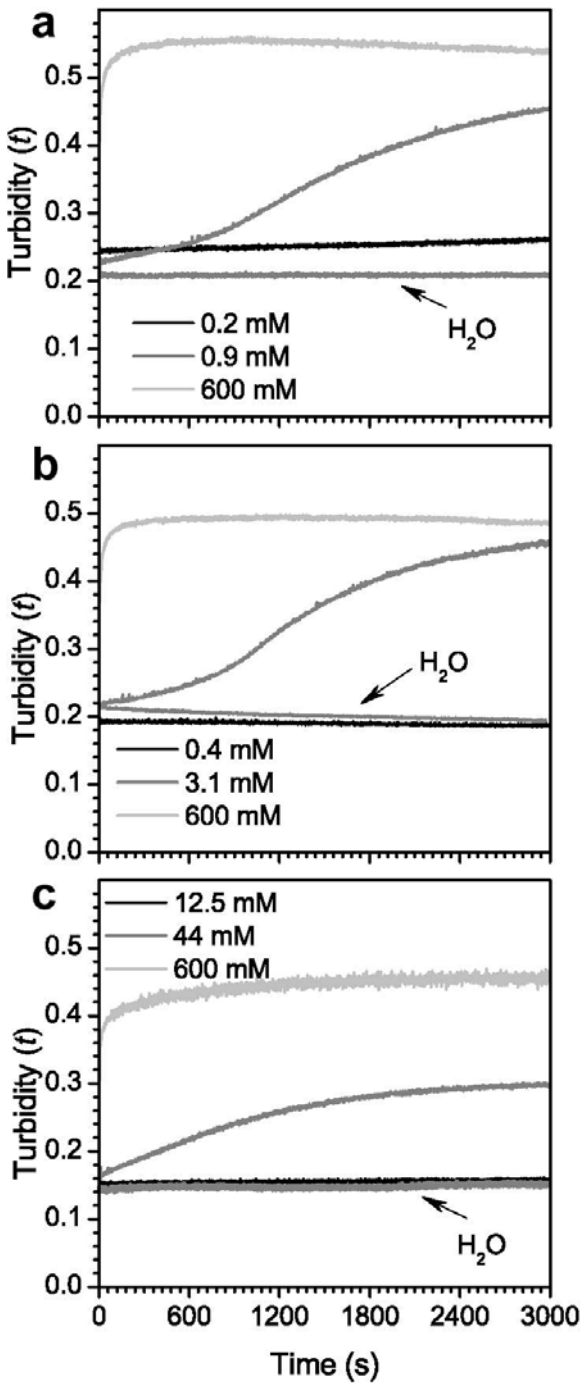

Figure 1. Changes in Accofloc® turbidity at 650 nm for 3000 s after addition of low, medium, and high concentrations of (a) $CaCl_2$, (b) $MgCl_2$, and (c) KCl. The turbidity value for Mg-montmorillonite in distilled water is shown.

Turbidity: three cases

Coagulation with three cation species, Ca^{2+}, Mg^{2+}, and K^+, was investigated. The coagulation dynamics in all experiments was divided into temporal subsets reflective of different aggregation states, *i.e.* linear growth and quasi-stable end point. Turbidity plots at λ = 650 nm for typical low, medium, and high concentrations of $CaCl_2$, $MgCl_2$, and KCl (Figure 1a–c) for 3000 s illustrate the transformations between the linear and rapid growth regions. The case of Mg-montmorillonite in distilled water is shown in Figure 1a.

For each cationic species, measurements fell into three groups: non-aggregating, slow-aggregating, and rapid aggregating. Turbidity increased for all the studied concentrations except over the lowest concentration ranges, indicative of growth in aggregate size. The time-evolution patterns of the turbidity exhibited one of three different configurations. In the lower cation concentration range (<0.2 mM $CaCl_2$; <0.4 mM $MgCl_2$; <12 mM KCl), τ remained constant over the 3000 s duration of the experiments, indicating a lack of aggregation. At slightly greater concentrations (second configuration), τ increased linearly over a period of several minutes to tens of minutes, after which τ increased more rapidly. At still more elevated concentrations, $\tau(t)$ exhibited linear behavior for a short interval after which τ rapidly approached its near-final (3000 s) value.

Early time/linear region

The brief duration of the linear growth region was considered an obstacle to turbidity measurements of aggregate growth rates (Puertas and Nieves, 1997). In the present exercise a wide range of cation concentrations was explored to provide an extended coverage of the linear growth region. During the initial post-mixing phase, aggregates produced were small ($kr << 1$) and N grew linearly with time (equation 3), leading to a linear increase in turbidity. The duration of this 'linear' region decreased as the cation concentration increased (Figure 2). The slope of the growth parameter, $\tau(t)$, over the linear period varied with both cation concentration and valence; increasing concentration drives the slope upscale until it reaches a saturation point. The linear region slope is plotted in Figure 3. Note that the slope of $\tau(t)$ is proportional to the aggregation rate and, therefore, proportional to the probability of particles adhering upon collision. This linear region behavior is consistent with the DLVO model. At reduced cation concentration, the diffuse layer of charge is thick and the potential barrier is substantially greater than k_BT. In this situation, aggregation is in the RLCA regime and aggregate growth rate is slow. At greater cation concentration, the double layer thickness was decreased, reducing the potential barrier height and resulting in an increased probability of platelets overcoming the barrier and adhering. Elevated cation concentration lowered the potential barrier, resulting in an increased sticking probability. At the CCC, the repulsive barrier is zero and every collision results in particle adhesion, *i.e.* the DLCA regime. Further increase in cation concentration above the CCC does not favor increased aggregation

https://doi.org/10.1346/CCMN.2013.0610101 Published online by Cambridge University Press

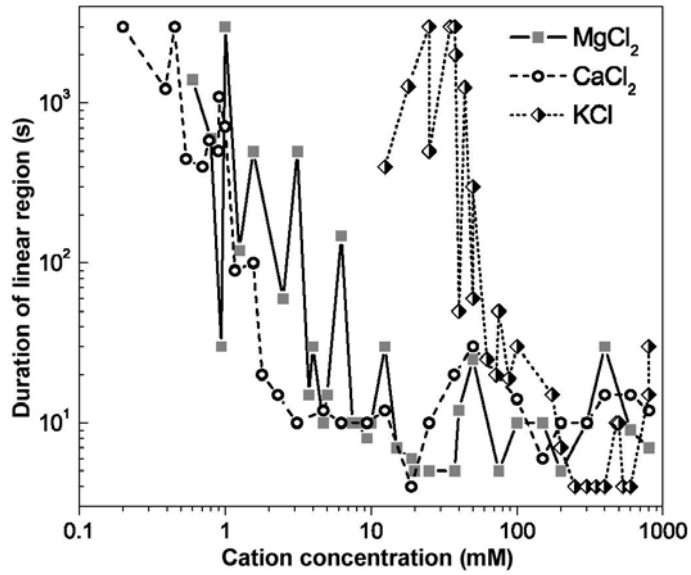

Figure 2. Duration of linear region.

rates. A CCC of 3 mM for $CaCl_2$, 4 mM for $MgCl_2$, and 70 mM for KCl was observed (Figure 3), in reasonable agreement with the Schulze-Hardy rule.

The stability ratio (W) was defined as the ratio of the number of total collisions to the number of collisions resulting in adhesion (Hunter, 1993). The ratio is equal to the reciprocal of the aggregation rate after normalizing the rate such that for concentrations greater than the CCC, the rate is unity. At the lowest concentrations for which aggregation was observed, the stability ratio was ~10^4 (Figure 4). A linear fit to the log-log data at concentrations below the CCC yielded slopes of -3.2 ± 0.7 for $CaCl_2$, -3.3 ± 0.4 for $MgCl_2$, and -6.7 ± 1.7 for KCl. The resulting monovalent to divalent slope ratio of ~2 indicates that the stability ratio varies as $1/z$ rather than the $1/z^2$ model proposed by Reerink and Overbeek (1954), where z represents cation valence. Experimental slope results frequently fail to follow the predicted $1/z^2$ relationship (Elimelech *et al*., 1998). The observed $1/z$ dependence appears to be a result of the non-spherical shape and the unique charge distribution found in clay platelets. These factors may result in

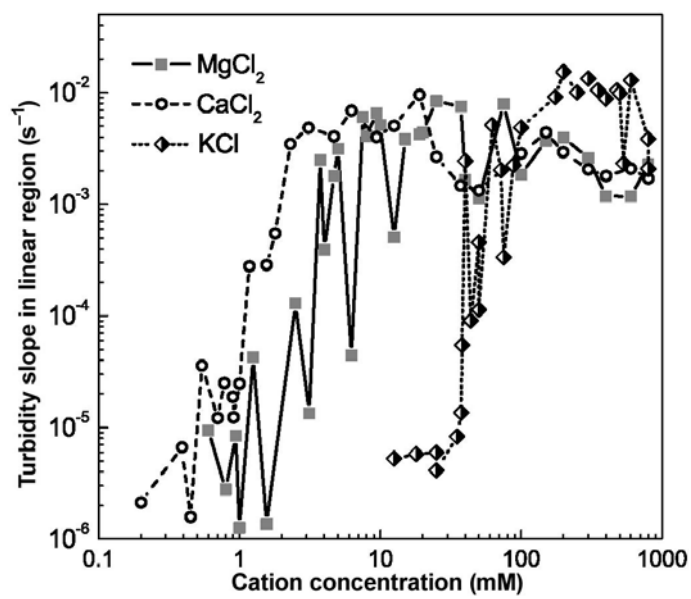

Figure 3. Slope of turbidity in linear growth region.

https://doi.org/10.1346/CCMN.2013.0610101 Published online by Cambridge University Press

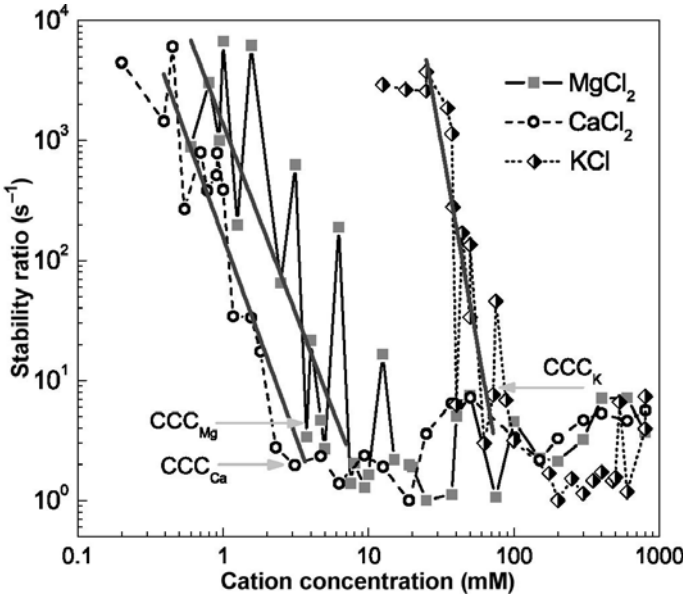

Figure 4. Stability ratios, CCC, are indicated.

different potential barriers for F-F, E-F, or E-E platelet associations. Czigany *et al*. (2005) also observed a departure from the $1/z^2$ model in montmorillonite, though the ratio of the stability slope in NaCl to $CaCl_2$ calculated by those authors was 0.5.

Later time/larger aggregates

For the three cations, the linear region transitioned ultimately into an equilibration interval characterized by a turbidity which is generally stable for most cation concentrations. That the turbidity remained relatively constant for the higher concentrations does not necessary imply that aggregate growth had discontinued. In the limit of large aggregate size, τ becomes approximately independent of r for $D_f < 2$ but increases as $\tau \propto r^{2-D_f}$ for $D_f > 2$. Thus, a constant turbidity can be used as an indicator that $D_f < 2$, *i.e.* aggregation is in the DLCA. This case allows the appropriate approximations of turbidity and forward scattering factors to be applied to the analysis of fractal dimension. From equation 4, in the limit $kr >> 1$, and $D_f < 2$ (DLCA), $\tau \propto k^{4-D_f}$ can be shown. For $D_f > 2$, τ becomes proportional to k^2; therefore, the fractal dimension can be extracted more readily from the turbidity spectrum for DLCA than for RLCA. The slopes of $\tau(k)$ at 3000 s (not corrected for forward scattering) for all studied cation concentrations are shown in Figure 5. At the greater cation concentrations (*i.e.* DLCA) the slope is <2, while for lower concentrations (*i.e.* RLCA) the slope is >2, demonstrating the necessity to correct the turbidity for forward scattering. For $kr >> 1$ and $D_f < 2$, the forward scattering correction factor was approximated as $\gamma \approx (\sin\theta/2)^{2-D_f}$ to simplify the correction to the turbidity. Under this assumption, D_f can be calculated directly from the turbidity. The fractal dimension for cation concentrations that satisfy these conditions are shown in Figures 6a–c. All concentrations above the CCC were characterized by $D_f < 2$. For cation levels at some degree below the CCC, $D_f < 2$. This indicates that although multiple collisions are needed for particle adhesion, the mass fractal dimension of the aggregate is more consistent with DLCA than RLCA. For the DLCA datasets, the Ca^{2+} and Mg^{2+} groups correspond to fractal dimensions of 1.65±0.3 and 1.75±0.3, respectively, except for the lowest concentrations. In contrast, the fractal dimension for the K^+-aggregated Mg-montmorillonite increased consistently from 1.35 to 1.95. This can be a consequence of a preponderance of the more loosely packed E-F and E-E associations in the aggregates at lower KCl concentrations, while the aggregates in the divalent cation suspensions were predominantly F-F associations. The differences in fractal characteristics between the monovalent and divalent cations can also be related to the effects of the cations on tactoid structure (Schramm and Kwak, 1982; Whalley and Mullins, 1991). Similar results were found by Tombácz and Szekeres (2004), who observed that montmorillonite formed E-F aggregates at concentrations above 25 mM NaCl and F-F aggregates above 100 mM NaCl at pH 4.

Notably, turbidity reached a maximum in tandem with concentration for the monovalent system whereas for the divalent system the turbidity maximum occurred at mid-level concentrations (Figure 7). This may be a consequence of increased water viscosity at very high cation concentrations and subsequent effects on aggregation. For the divalent cations at concentrations greater than the CCC, D_f is independent of cation concentration

https://doi.org/10.1346/CCMN.2013.0610101 Published online by Cambridge University Press

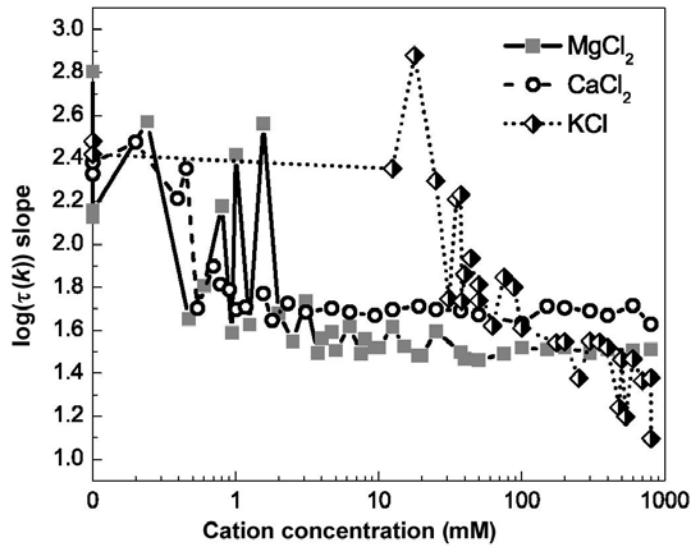

Figure 5. Slope of log–log plot of $\tau(k)$ at 3000 s. τ is not corrected for forward scattering.

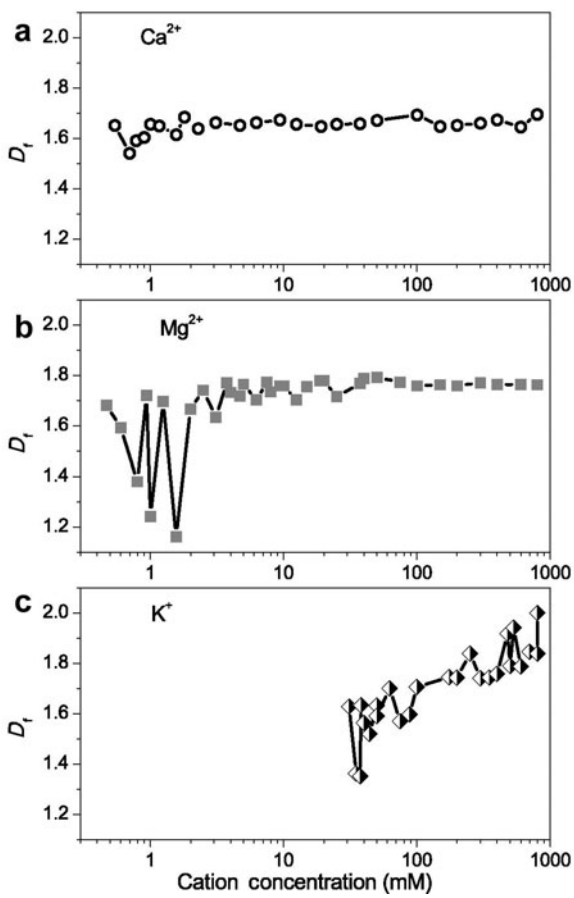

Figure 6. Aggregate fractal dimension as a function of cation concentration at $t = 3000$ s for (a) Ca^{2+}, (b) Mg^{2+}, and (c) K^{+}.

and, therefore, from equation 4, the greater turbidity associated with mid-level concentration of divalent cations implies that aggregate size is greater at mid-concentration. This is in contrast to the monovalent cation in which the largest aggregates occur at elevated K^{+} concentrations.

An unusual feature of KCl aggregation relates to differences in the temporal location of the maximum turbidity. For the mid-level concentrations (100−500 mM), τ_{max} occurs at an early time (<10 min) but for high-level concentrations (>500 mM), τ_{max} is found at the end of the experiment (50 min, Figure 8). This may indicate that at mid-level K^{+} concentrations, either the flocs exhibit a degree of partial disaggregation or a decrease in D_f over time, a result not observed in divalent experiments.

CONCLUSION

An improved understanding of the conditions necessary for the consolidation of cohesive smectite aggregates is of great importance to environmental and industrial concerns. The baseline for the conditions where flocculation is induced has been established here through an analysis of turbidity measurements in the linear growth region. These values were employed to determine relative aggregation rates, the relevant stability ratios for aggregate growth, and a working definition for the CCC range.

A key finding of this investigation pertains to a comparison of the stability ratio of the log-log slope for the divalent cations relative to the monovalent case which shows that smectite aggregation rates differ substantially from those implied by DLVO theory. This indicates that the impact of plate-like geometry in a natural system produces a condition that is less sensitive

https://doi.org/10.1346/CCMN.2013.0610101 Published online by Cambridge University Press

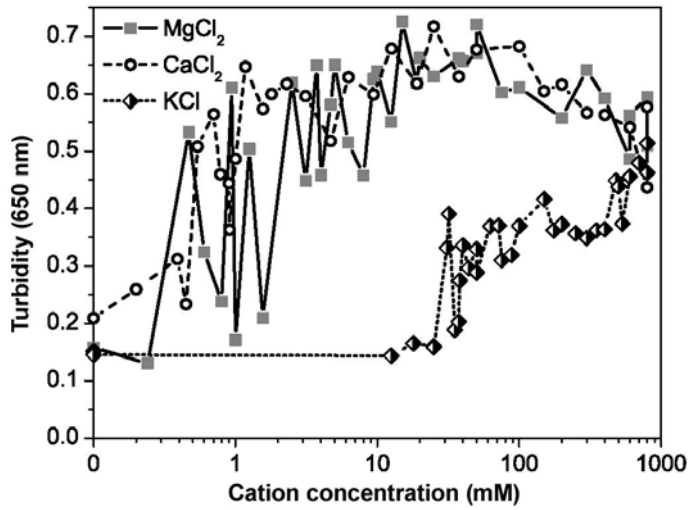

Figure 7. Turbidity at 3000 s after addition of cations.

to cation valence than in idealized experiments conducted with spherical primary particles. The DLVO theory was also found (Missana and Adell, 2000) to be unable to accurately predict clay colloidal stability, a result of pH-dependent charge distribution and the role of edge-to-face effects in aggregation.

The CCC is considered the boundary condition that separates rapid from slow aggregation rates where the rapid condition corresponds to DLCA and the slow condition to RLCA. This data set demonstrates that for a range of concentrations below the CCC the DLCA regime prevails. This is expected to hold true for different homoionic clay minerals (Na^+, K^+, or Ca^{2+}), although variation in surface charge may result in a different CCC value. Greater fractal dimension at greater cation concentration indicates more F-F associations, while lower cation concentration appears to favor E-F and E-E platelet associations. The greater effectiveness of divalent cations on aggregation has a bearing on the coalescence of particulate aggregates in systems with significant variations in the flux of dissolved species, such as estuaries and lacustrine environments and in areas subject to upward migrations of water through pore solutions.

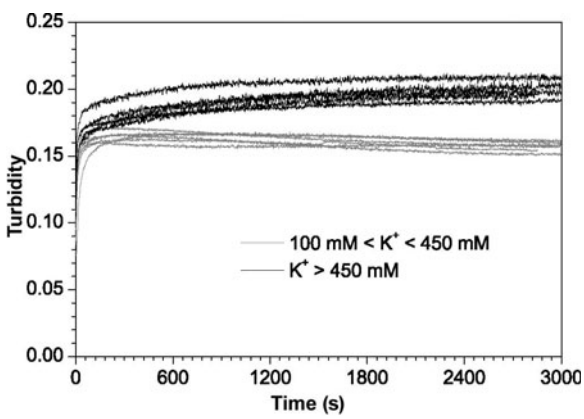

Figure 8. Turbidity at mid- and high-level concentrations of K^+.

ACKNOWLEDGMENTS

The present work was supported in part by a City Seed grant #93370-09 from the City College of New York, PSC-CUNY Award #64577-00 42, and an NIH Research Centers in Minority Institutions (NIH/NCRR/RCMI) CCNY/Grant G12-RR03060.

REFERENCES

Alimova, A., Katz, A., Orozco, J., Wei, H., Gottlieb, P., Rudolph, E., Steiner, J.C., and Xu, M. (2009) Time evolution of smectite fractal dimension measured by broadband light scattering. *Journal of Optics A: Pure and Applied Optics*, **11**, 105706.

Banin, A. and Lahav, N. (1968) Optical study of particle size of montmorillonite with various adsorbed cations. *Nature*, **217**, 1146–1147.

Berka, M. and Rice, J.A. (2004) Absolute aggregation rate constants in aggregation of kaolinite measured by simultaneous static and dynamic light scattering. *Langmuir*, **20**, 6152–6157.

Berka, M. and Rice, J.A. (2005) Relation between aggregation kinetics and the structure of kaolinite aggregates. *Langmuir*, **21**, 1223–1229.

Berry, M.V. and Wills, H.H. (1986) Optics of fractal clusters such as smoke. *Optica Acta*, **33**, 577–591.

Bouchelaghem, F. and Jozja, N. (2009) Multi-scale study of permeability evolution of a bentonite clay owing to pollutant transport: Part I. Model derivation. *Engineering Geology*, **108**, 119–132.

Czigany, S., Flury, M., and Harsh, J.B. (2005) Colloid stability in vadose zone Hanford sediments. *Environmental Science & Technology*, **39**, 1506–1512.

Derjaguin, B. and Landau, L. (1941) Theory of the stability of strongly charged lyophobic sols and of the adhesion of strongly charged particles in solution of electrolytes. *Acta Physicochimica*, **14**, 633–662.

https://doi.org/10.1346/CCMN.2013.0610101 Published online by Cambridge University Press

Derrendinger, L. and Sposito, G. (2000) Flocculation kinetics and cluster morphology in illite/NaCl suspensions. *Journal of Colloid and Interface Science*, **222**, 1–11.

Elimelech, M., Gregory, J., Jia, X., and Williams, R. (1998) *Particle Deposition and Aggregation: Measurement, Modelling and Simulation*. Butterworth-Heinemann, London.

Ferreiro, E.A. and Helmy, A.K. (1974) Flocculation of Na-montmorillonite by electrolytes. *Clays and Clay Minerals*, **10**, 203–213.

García-García, S., Jonsson, M., and Wold, S. (2006) Temperature effect on the stability of bentonite colloids in water. *Journal of Colloid and Interface Science*, **298**, 694–705.

García-García, S., Wold, S., and Jonsson, M. (2007) Kinetic determination of critical coagulation concentrations for sodium- and calcium-montmorillonite colloids in NaCl and $CaCl_2$ aqueous solutions. *Journal of Colloid and Interface Science*, **315**, 512–519.

Goldberg, S., Forster, H.S., and Heick, E.L. (1991) Flocculation of illite/kaolinite and illite/montmorillonite mixtures as affected by sodium adsorption ratio and pH. *Clays and Clay Minerals*, **39**, 375–380.

Goldberg, S. and Glaubig, R.A. (1987) Effect of saturating cation, pH, and aluminum and iron oxide on the flocculation of kaolinite and montmorillonite. *Clays and Clay Minerals*, **35**, 220–227.

Hunter, R.J. (1993) *Introduction to Modern Colloid Science*. Oxford University Press, New York, 344 pp.

Keren, R. and Sparks, D.L. (1995) The role of edge surfaces in flocculation of 2:1 clay minerals. *Soil Science Society of America Journal*, **59**, 430–435.

Kobayashi, M. and Ishibashi, D. (2011) Absolute rate of turbulent coagulation from turbidity measurement. *Colloid & Polymer Science*, **289**, 831–836.

Kornilovich, B., Mishchuk, N., Abbruzzese, K., Pshinko, G., and Klishchenko, R. (2005) Enhanced electrokinetic remediation of metals-contaminated clay. *Colloids and Surfaces A: Physicochemical and Engineering Aspects*, **265**, 114–123.

Lagaly, G. (2006) Colloid Clay Science. Pp. 141–246 in: *Handbook of Clay Science*, **1** (F. Bergaya, B.K.G. Theng, and G. Lagaly, editors). Elsevier, Amsterdam.

Lagaly, G. and Ziesmer, S. (2003) Colloid chemistry of clay minerals: the coagulation of montmorillonite dispersions. *Advances in Colloid and Interface Science*, **100–102**, 105–128.

Lin, M.Y., Lindsay, H.M., Weitz, D.A., Ball, R.C., Klein, R., and Meakin, P. (1989) Universality in colloid aggregation. *Nature*, **339**, 360–362.

Lin, M.Y., Lindsay, H.M., Weitz, D.A., Ball, R.C., Klein, R., and Meakin, P. (1990a) Universal reaction-limited colloid aggregation. *Physical Review A*, **41**, 2005–2030.

Lin, M.Y., Lindsay, H.M., Weitz, D.A., Klein, R., Ball, R.C., and Meakin, P. (1990b) Universal diffusion-limited colloid aggregation. *Journal of Physics: Condensed Matter*, **2**, 3093–3113.

Luckham, P.F. and Rossi, S. (1999) The colloidal and rheological properties of bentonite suspensions. *Advances in Colloid and Interface Science*, **82**, 43–92.

Meakin, P. (1983) Formation of fractal clusters and networks by irreversible diffusion-limited aggregation. *Physical Review Letters*, **51**, 1119–1122.

Missana, T. and Adell, A. (2000) On the applicability of DLVO theory to the prediction of clay colloids stability. *Journal of Colloid and Interface Science*, **230**, 150–156.

Moore, D. and Reynolds, R.C., Jr. (1997) *X-ray Diffraction and the Identification and Analysis of Clay Minerals*, 2nd edition. Oxford University Press, New York.

Morris, G.E. and Żbik, M.S. (2009) Smectite suspension structural behaviour. *International Journal of Mineral Processing*, **93**, 20–25.

Nasser, M.S. and James, A.E. (2009) The effect of electrolyte concentration and pH on the flocculation and rheological behaviour of kaolinite suspensions. *Journal of Engineering Science and Technology*, **4**, 430–446.

Novich, B.E. and Ring, T.A. (1984) Colloid stability of clays using photon correlation spectroscopy. *Clays and Clay Minerals*, **32**, 400–406.

Pierre, A.C. and Ma, K. (1999) DLVO theory and clay aggregate architectures formed with $AlCl_3$. *Journal of the European Ceramic Society*, **19**, 1615–1622.

Plaschke, M., Schäfer, T., Bundschuh, T., Ngo Manh, T., Knopp, R., Geckeis, H., and Kim, J.I. (2001) Size characterization of bentonite colloids by different methods. *Analytical Chemistry*, **73**, 4338–4347.

Ploehn, H.J. and Liu, C. (2006) Quantitative analysis of montmorillonite platelet size by atomic force microscopy. *Industrial & Engineering Chemistry Research*, **45**, 7025–7034.

Puertas, A.M. and Nieves, F.J.d.l. (1997) A new method for calculating kinetic constants within the Rayleigh – Gans – Debye approximation from turbidity measurements. *Journal of Physics: Condensed Matter*, **9**, 3313.

Ravera, M., Ciccarelli, C., Gastaldi, D., Rinaudo, C., Castelli, C., and Osella, D. (2006) An experiment in the electro-kinetic removal of copper from soil contaminated by the brass industry. *Chemosphere*, **63**, 950–955.

Reerink, H. and Overbeek, J.T.G. (1954) The rate of coagulation as a measure of the stability of silver iodide sols. *Discussions of the Faraday Society*, **18**, 74–84.

Schramm, L.L. and Kwak, J.C.T. (1982) Influence of exchangeable cation composition on the size and shape of montmorillonite particles in dilute suspension. *Clays and Clay Minerals*, **30**, 40–48.

Sorensen, C.M. (2001) Light scattering by fractal aggregates: a review. *Aerosol Science & Technology*, **35**, 648–687.

Spinrad, R.W., Zaneveld, J.R.V., and Pak, H. (1978) Volume scattering function of suspended particulate matter at near-forward angles: a comparison of experimental and theoretical values. *Applied Optics*, **17**, 1125–1130.

Środoń, J. (2006) Identification and quantitative analysis of clay minerals. Pp. 765–788 in: *Handbook of Clay Science*, **1** (F. Bergaya, B.K.G. Theng, and G. Lagaly, editors) Elsevier, Amsterdam.

Stawiński, J., Wierzchoś, J., and Garcia-Gonzalez, M.T. (1990) Influence of calcium and sodium concentration on the microstructure of bentonite and kaolin. *Clays and Clay Minerals*, **38**, 617–622.

Tawari, S.L., Koch, D.L., and Cohen, C. (2001) Electrical double-layer effects on the Brownian diffusivity and aggregation rate of Laponite clay particles. *Journal of Colloid and Interface Science*, **240**, 54–66.

Tombácz, E. and Szekeres, M. (2004) Colloidal behavior of aqueous montmorillonite suspensions: the specific role of pH in the presence of indifferent electrolytes. *Applied Clay Science*, **27**, 75–94.

Tournassat, C., Neaman, A., Villiéras, F., Bosbach, D., and Charlet, L. (2003) Nanomorphology of montmorillonite particles: Estimation of the clay edge sorption site density by low-pressure gas adsorption and AFM observations. *American Mineralogist*, **88**, 1989–1995.

van Olphen, H. (1977) *Introduction to Clay Colloid Chemistry*. Wiley-Interscience Publication, John Wiley & Sons, New York.

van Oss, C.J., Giese, R.F., and Costanzo, P.M. (1990) DLVO and non-DLVO interactions in hectorite. *Clays and Clay Minerals*, **38**, 151–159.

Verwey, E.J.W. and Overbeek, J.T.G. (1948) *Theory of the Stability of Lyophobic Colloids*. Elsevier Publishing, New York.

von Wachenfeldt, E., Bastviken, D., and Tranvik, L.J. (2009) Microbially induced flocculation of allochthonous dissolved organic carbon in lakes. *Limnology and Oceanography*, **54**, 1811–1818.

Whalley, W.R. and Mullins, C.E. (1991) Effect of saturating cation on tactoid size distribution in bentonite suspensions. *Clay Minerals*, **26**, 11–17.

Wind, L. and Szymanski, W.W. (2002) Quantification of scattering corrections to the Beer-Lambert law for transmittance measurements in turbid media. *Measurement Science and Technology*, **13**, 270.

(*Received 12 July 2012; revised 19 December 2012; Ms. 691; AE: S. Wold*)